Nanoscale

PAPER

View Article Online
View Journal

Cite this: DOI: 10.1039/d1nr00792k

Construction of 3D Bi/$ZnSnO_3$ hollow microspheres for label-free highly selective photoelectrochemical recognition of norepinephrine†

Yuanyuan Dong,[a,b] Chenxing Xu[a] and Lei Zhang *[a]

Received 5th February 2021,
Accepted 1st April 2021

DOI: 10.1039/d1nr00792k

rsc.li/nanoscale

Herein, we reported a label-free and reliable photoelectrochemical (PEC) platform for highly selective monitoring of norepinephrine (NE) based on metallic Bi nanoparticles anchored on hollow porous $ZnSnO_3$ microspheres (3D Bi/$ZnSnO_3$) *via* a simple solvothermal strategy. The designed 3D Bi/$ZnSnO_3$ Schottky junction exhibited a unique photoanodic response toward NE among other catechol derivatives, such as epinephrine (EP) and dopamine (DA), and effectively shielded the interference from thirteen coexisting biomolecules like uric acid (UA) and ascorbic acid (AA). High selectivity and excellent sensitivity could be correlated to the unique chelating coordination interaction between NE and Zn^{2+} at surface sites as well as the efficient carrier separation of Bi/$ZnSnO_3$, thereby developing a novel "signal-on" label-free and selective strategy for NE detection. The proposed Bi/$ZnSnO_3$-based PEC sensor achieved remarkable NE biosensing with a low detection limit of 0.68 nmol L^{-1} and a wide response ranging from 0.002 to 350.0 μmol L^{-1}. The applicability of this biosensor was realized for the selective analysis of NE in human serum, human urine and injection samples, laying the foundation for the label-free PEC monitoring of NE in biological fluids.

1. Introduction

Photoelectrochemical (PEC) biosensing, as an advanced detection technique, has attracted extensive research interest in the bioanalysis and medicine analysis fields, and offers higher sensitivity and lower background signal than conventional electrochemical sensors due to the separation of photoexcitation and detection signals.[1,2] Portability, simple equipment, rapid detection, high precision and cost-effectiveness are the featured characteristics of PEC biosensors. However, it is generally accepted that the broad PEC reaction on the photoelectrode impedes the selectivity of many PEC systems.[3,4] To resolve this problem, molecular recognition units such as enzymes,[5] antibodies[6] and aptamers[7] have been introduced into the sensing system. However, the introduction of additional recognition units is not only costly, but also time-consuming. An effective strategy is the use of unique bonding interactions between the photoelectrode and the target, resulting in the improvement of selectivity and recognition ability. For instance, Zhang *et al.* prepared an AgI/$CuBi_2O_4$ heterojunction to selectively detect L-cysteine, based on the formation of Cu–S and Ag–S bonds.[8] Wang *et al.* have constructed a "signal-off" PEC sensor based on the I-BiOCl/N-GQD composite for the selective detection of chlorpyrifos owing to the coordination of surface Bi^{3+} with chlorpyrifos.[9] Thus, exploring recognition unit-free PEC biosensors is one of the main goals of the present study.

Norepinephrine (NE) is one of the essential catecholamine neurotransmitters in the mammalian central nervous systems. NE in the medical field is able to treat bronchial asthma, heart attacks and hypertension.[10–12] Abnormal concentrations of NE are closely related to several adverse reactions, including ganglia neuroblastoma, congestive arrhythmias and Parkinson's disease.[13,14] Hence, accurately monitoring the concentration of NE is very important. However, the oxidation signal of NE is commonly interfered with by those of other biomolecules coexisting in biological systems, particularly DA, AA and amino acids, because they have similar characteristics and structural features, and can be oxidized at close potentials. Consequently, developing an accurate, sensitive and selective method for the quantitative detection of NE in biological fluids is an urgent priority.[15,16] Coincidentally, it has been found that Zn-containing compounds can readily coordinate with the catechol structure to form a steady chelate.[17] Maikap

[a]College of Chemistry, Liaoning University, 66 Chongshan Middle Road, Shenyang, Liaoning, 110036, People's Republic of China. E-mail: zhanglei63@126.com; Tel: +8624 62207809; Fax: +86 24 62202380
[b]College of Materials and Chemical Engineering, Heilongjiang Institute of Technology, Harbin, 150050, People's Republic of China

†Electronic supplementary information (ESI) available. See DOI: 10.1039/d1nr00792k

et al. proposed a ZnO-based nonenzymatic electrochemical sensor for the selective detection of catechol, confirming the strong electrochemical interaction between the catechol and the ZnO thin film.[18] Sakthinathan *et al.* demonstrated that the strong coordination interaction between Zn^{2+} and –OH could promote the selective adsorption of DA based on an RGO/Zn-TPP-modified electrode.[19] Therefore, it is not only a great challenge to design high-efficiency Zn-based photoelectroactive materials for selective sensing of NE, but also difficult to achieve accurate discrimination of NE among various catechol derivatives.

At present, extensive efforts have been made to promote the PEC activity of photoelectroactive materials. For instance, the PEC performance can be improved by appropriately designing, doping and combining them with metals or other semiconductors to form heterostructures.[20–23] It is worth noting that it is difficult for the semiconductor–semiconductor heterojunction to achieve strong redox capability and effective electron–hole separation simultaneously due to the accumulation of photo-generated carriers in the band with lower redox potentials.[24] Recently, the metal/semiconductor Schottky junction has attracted considerable attention owing to its perfect role in improving the PEC performance, which can not only promote surface charge separation, but also form a Schottky barrier that can also act as an effective electron trap to inhibit the electron–hole pair recombination, and effectively preserve excellent redox ability.[25,26]

Inspired by these factors, metallic Bi nanoparticles were modified on the surface of hollow $ZnSnO_3$ microspheres to form a Schottky junction for the label-free PEC determination of NE. The original architecture holds many attractive features including a tight heterostructure interface, plentiful charge transport channels, large contactable area and numerous active sites for surface reactions. Based on the specific chelating interaction and controlling the bias potential, the developed PEC platform could highly sensitively recognize NE among various catechol derivatives and shield other coexisting biomolecules. Meanwhile, the possible mechanism of excellent sensitivity and selectivity of the developed PEC platform was also proposed and adequately explored. More importantly, this research provided a new idea for the design of the PEC sensing platform by considering the composition and interaction with targets.

2. Experimental

2.1 Materials and reagents

Zinc nitrate hexahydrate ($Zn(NO_3)_2{\cdot}6H_2O$), tin tetrachloride pentahydrate ($SnCl_4{\cdot}5H_2O$), sodium hydroxide (NaOH), bismuth nitrate ($Bi(NO_3)_3{\cdot}5H_2O$), sodium sulfate (Na_2SO_4) and ethylene glycol (EG) were bought from Sinopharm Chemical Reagent Co., Ltd (Shenyang, China). Polyvinyl pyrrolidone (PVP, K30) and norepinephrine (NE) were purchased from Aladdin Biological Co., Ltd (Shanghai, China). All chemicals used were of analytical grade and used without any further purification.

2.2 Instruments

The composition and microstructures of the obtained samples were characterized by scanning electron microscopy (SEM, HITACHI, SU8000, Japan), equipped with energy dispersive X-ray spectroscopy (EDS). The microstructures were observed under a transmission electron microscope (TEM, JEOL JEM-2100, Japan). The crystalline phase of the samples was characterised using a Siemens D5000 X-ray diffractometer (XRD, Germany). Fourier transform infrared (FT-IR) spectra were acquired with a Nicolet 330 spectrometer (Nicolet, USA). UV-vis diffuse reflection spectra (DRS) were recorded on a Shimadzu UV-2550 spectrophotometer (Japan). Photoluminescence emission spectra (PL) were recorded on the F-7000 spectrophotometer (Hitachi High Technologies, Japan) with an excitation wavelength of 298 nm.

2.3 Material synthesis

The $ZnSnO_3$ hollow microspheres were prepared by an easy one-pot template-free method and are described as follows. Briefly, 6.0 mmol $Zn(NO_3)_2{\cdot}6H_2O$, 6.0 mmol $SnCl_4{\cdot}5H_2O$ and 60.0 mmol NaOH were dissolved in water–ethanol solution (140.0 mL, volume ratio was 2 : 1) with vigorous agitation for 20 min. Meanwhile, 150.0 mmol NaOH was dispersed in 40.0 mL water–ethanol solution and slowly added dropwise to the above solution to form a white suspension. After stirring for 15 min, the suspension was transferred to the water bath and heated under reflux at 80 °C for 3 h. Then, the white precipitate was harvested by centrifugation and then rinsed repeatedly with deionized water and ethanol, and dried at 60 °C overnight. Finally, the precursor was annealed at 400 °C for 2 h to get the final product of $ZnSnO_3$ microspheres.

The $Bi/ZnSnO_3$ composites were prepared by a typical solvothermal method. Firstly, 0.75 mmol $Bi(NO_3)_3{\cdot}5H_2O$ was dissolved in 10.0 mL of HNO_3 solution (1.0 mol L^{-1}) with intensive stirring, followed by the addition of 55.0 mL of EG and 0.6 g of PVP until a clear solution was obtained. After that, a certain amount of the pre-synthesized $ZnSnO_3$ powders was added. After 10 min, the mixture was transferred into a 100.0 mL Teflon-lined stainless steel autoclave and heated at 150 °C for 12 h. The products were collected by centrifugation, washing and drying at 60 °C. By changing the mass of the $ZnSnO_3$ added, three $Bi/ZnSnO_3$ samples with different Bi mass ratios (20, 30 and 40 wt%) were fabricated, and the resulting samples were denoted as $Bi/ZnSnO_3$-1, $Bi/ZnSnO_3$-2, and $Bi/ZnSnO_3$-3, respectively. In addition, pure Bi nanoparticles were also synthesized using the same method in the absence of $ZnSnO_3$.

2.4 Fabrication of PEC biosensor

Fluoride doped tin oxide glass (FTO) was pre-treated as follows: the FTO substrate (1 cm × 2 cm) was successively cleaned ultrasonically in acetone, ethanol and distilled water for 30 min, respectively, and then dried under an infrared

lamp for use. 3.0 mg of the Bi/$ZnSnO_3$-2 powder were ultrasonically dispersed in 0.5 mL of distilled water and subsequently drop-casted on the cleaned FTO electrode with an area of 1.0 cm^2, and dried naturally. The modified electrode was denoted as Bi/$ZnSnO_3$-2/FTO. As a contrast, Bi/$ZnSnO_3$/FTO with different ratios of metallic Bi was fabricated using the same method.

2.5 PEC measurements

All PEC experiments were performed on a CHI660D electrochemical workstation (Chenhua Instrument Co., Shanghai, China), which was connected with a classic three electrode system including a modified FTO as a working electrode, a Pt wire as the opposite electrode and a saturated calomel electrode (SCE) as the reference electrode. The transient photocurrents were determined by the i-t technique for several on–off cycles of light irradiation in a 0.1 mol L^{-1} Na_2SO_4 electrolyte solution at a bias potential of 0.5 V (*vs.* SCE); a 300 W xenon lamp (λ > 420 nm, Perfect Technology Co. Ltd, China) was used as a light source. Electrochemical impedance spectroscopy (EIS) was performed under the dark and light conditions at an open circuit potential, with a frequency swept from 0.1 to 10 kHz in a 1.0 mmol L^{-1} $[Fe(CN)_6]^{3-/4-}$ solution containing 1.0 mol L^{-1} KCl.

3. Results and discussion

3.1 Structural and morphological characteristics

The Bi/$ZnSnO_3$ Schottky junction was prepared *via* a two-step growth process. Firstly, $ZnSnO_3$ microspheres were synthesized by a template-free strategy. The representative SEM images in Fig. 1A and B indicate that the diameter of the $ZnSnO_3$ microspheres was about 700–900 nm, revealing that the surface of the $ZnSnO_3$ microspheres was highly coarse and composed of many irregular nanoparticles. The broken microsphere image in Fig. 1B and the TEM image in Fig. 1C clearly presented a porous hollow structure. After the solvothermal reaction, many Bi nanoparticles were observed to adhere tightly to the surface of $ZnSnO_3$ microspheres, as shown in Fig. 1D and E. It could be seen that the hollow structure of the microsphere was well preserved. The individual TEM image (Fig. 1F) revealed the darker surface edges of the microsphere, which was ascribed to the filling of the surface spaces by Bi nanoparticles during the synthesis process. A closer observation of the HRTEM image is shown in Fig. 1F, inset. The fringes with a lattice spacing of 0.328 and 0.238 nm could be indexed to (012) and (104) planes of Bi, further confirming that Bi nanoparticles were decorated on the surface of $ZnSnO_3$ microspheres. Fig. S1A–C† shows the SEM images of the Bi/$ZnSnO_3$ samples decorated with different Bi contents. When the mass ratio was increased to 40 wt%, the microspheres were covered by a large number of nanoparticles. Moreover, the EDS images (Fig. S1D–F†) showed the presence of elements Zn, Sn, O and Bi in the Bi/$ZnSnO_3$ materials, and the results also revealed that the final mass contents of Bi in the three composites were approximately 21.42, 30.21 and 40.04 wt%.

Fig. 2A shows the XRD patterns of $ZnSnO_3$ and the Bi/$ZnSnO_3$ composites. All peaks were extremely narrow and sharp, indicating that all samples had excellent crystallinity. All of the diffraction peaks in the XRD patterns of the Bi/$ZnSnO_3$ samples could be indexed to the $ZnSnO_3$ perovskite (JCPDS card no. 11-0247) and the rhombohedral Bi (JCPDS card no. 44-1246) without shifts of positions, suggesting the successful formation of Bi/$ZnSnO_3$ composites. Moreover, the diffraction peak intensity of the metallic Bi became more obvious and strengthened with the increase of the Bi content. No other crystalline phases were observed in all of the patterns, indicating that the synthesized samples were of good purity. In the Raman spectra (Fig. 2B), two characteristic peaks

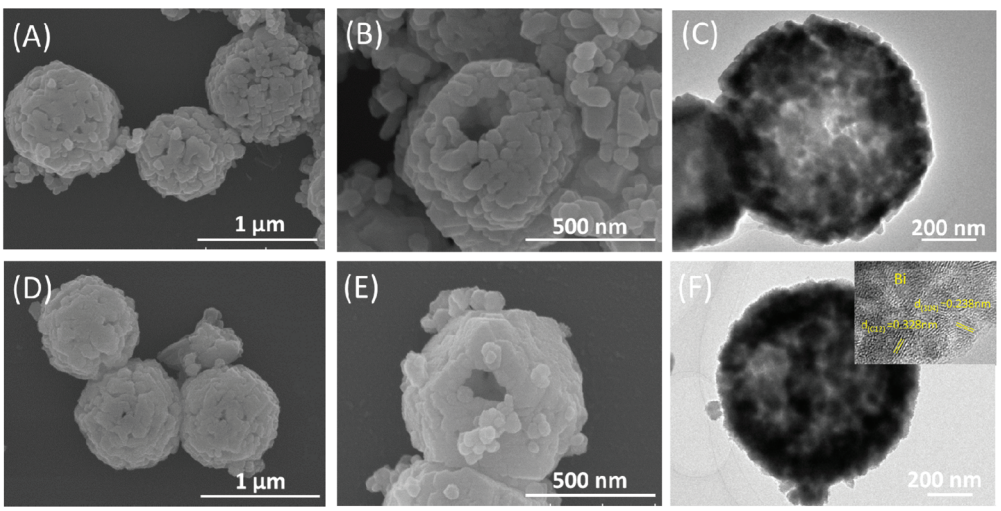

Fig. 1 Typical SEM (A, B) and TEM (C) images of $ZnSnO_3$ hollow microspheres; SEM (D, E), TEM (F) and HRTEM (inset) images of the as-prepared Bi/$ZnSnO_3$-2 samples.

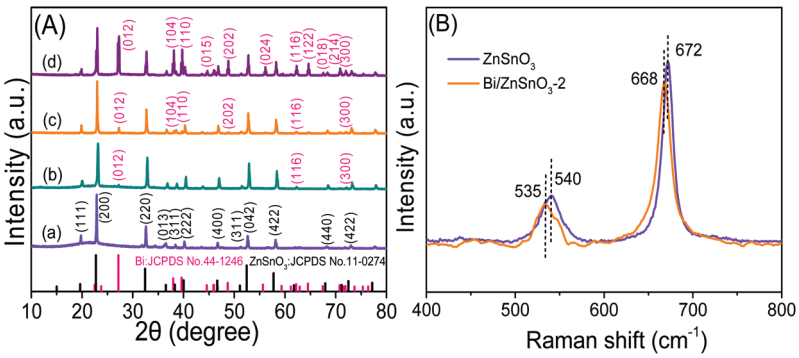

Fig. 2 (A) XRD patterns of (a) $ZnSnO_3$, (b) $Bi/ZnSnO_3$-1, (c) $Bi/ZnSnO_3$-2 and (c) $Bi/ZnSnO_3$-3 composites; (B) Raman spectra of $ZnSnO_3$ and $Bi/ZnSnO_3$-2 composites.

at 540 and 672 cm^{-1} were assigned to pure $ZnSnO_3$. The peak located at 540 cm^{-1} was related to the internal vibration of the oxygen tetrahedron, while the other strong peak at 672 cm^{-1} was attributed to the typical Raman shift of $ZnSnO_3$.[27] It is worth noting that a significant red-shift in the characteristic peaks of $ZnSnO_3$ was observed in the $Bi/ZnSnO_3$ samples after the introduction of metallic Bi, accompanied by a slight decrease in intensity. The results demonstrate the electron transfer and the interaction between the metallic Bi and $ZnSnO_3$ at the interface,[28,29] indicating the successful formation of the $Bi/ZnSnO_3$ Schottky junction.

3.2 Optical characteristics

UV-vis DRS were collected to study the optical properties of the synthesized samples. As illustrated in Fig. 3A, pure $ZnSnO_3$ showed a strong absorption edge at 397 nm owing to the intrinsic bandgap absorption.[30] When the metallic Bi was decorated on $ZnSnO_3$, the light-harvesting property of the $Bi/ZnSnO_3$ composite was apparently improved ranging from the UV light (200 nm) to near-infrared light (800 nm). In the visible light region, the absorption curves of the $Bi/ZnSnO_3$ samples strengthened in parallel with increasing the amount

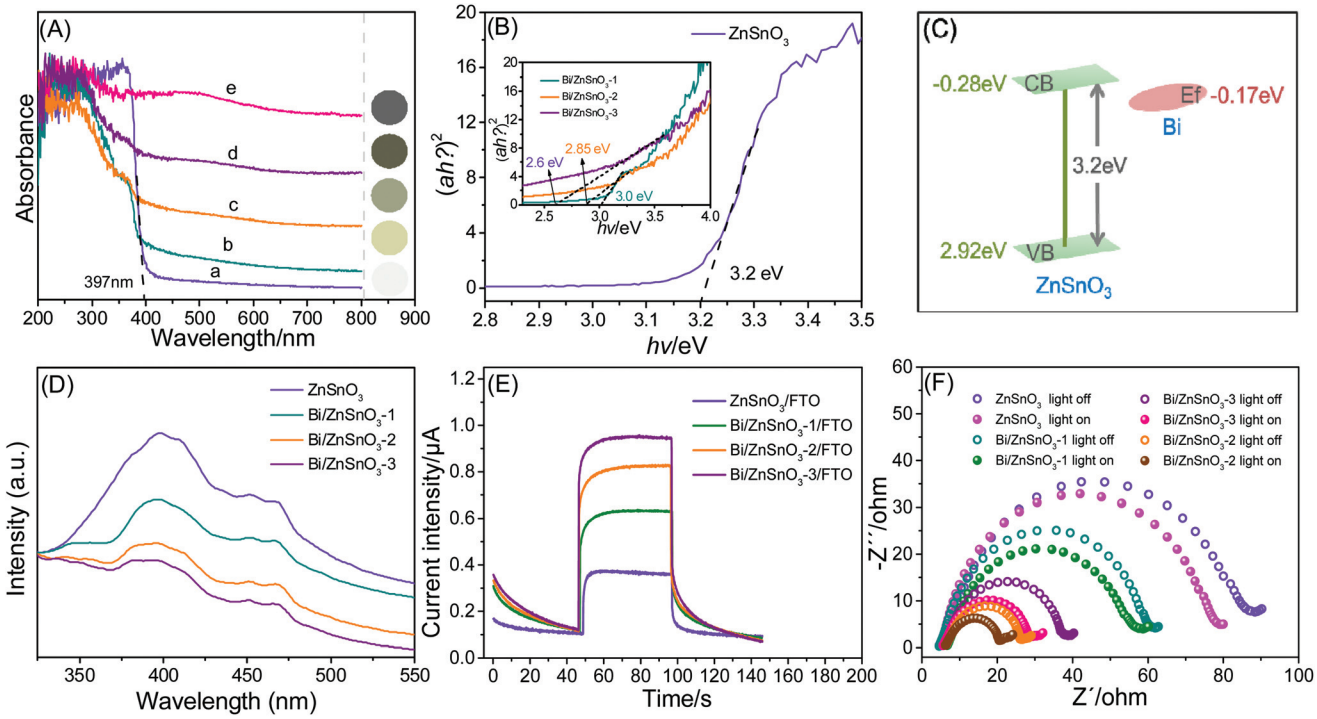

Fig. 3 (A) UV-Vis DRS spectra of (a) pure $ZnSnO_3$, (b) $Bi/ZnSnO_3$-1, (c) $Bi/ZnSnO_3$-2, (d) $Bi/ZnSnO_3$-3 and (e) metallic Bi; (B) plots of $(ahv)^2$ *vs.* photon energy (hv) for $ZnSnO_3$ and $Bi/ZnSnO_3$ composites (inset); (C) the energy band diagram of $ZnSnO_3$ and Bi (*vs.* NHE); (D) PL spectra of $ZnSnO_3$ and $Bi/ZnSnO_3$ composites; (E) photocurrent responses of $ZnSnO_3$/FTO and different $Bi/ZnSnO_3$/FTO samples recorded in 0.1 mol L^{-1} Na_2SO_4; (F) EIS spectra of $ZnSnO_3$/FTO and different $Bi/ZnSnO_3$/FTO samples under dark and illumination conditions.

of metallic Bi, which is in accordance with their color change from white to dark gray. Furthermore, an obvious SPR absorption at 200–400 nm could be easily observed owing to the SPR effect of the metallic Bi.[31,32] Undoubtedly, the introduction of metallic Bi was crucial for photo-exciting more electron–hole pairs to enhance the PEC activity of the Bi/$ZnSnO_3$ composites. In addition, the band gap value (E_g) of $ZnSnO_3$ was determined to be approximately 3.2 eV by fitting the relationship between $(ahv)^2$ and hv (Fig. 3B). Moreover, it was obvious that the E_g values of the Bi/$ZnSnO_3$ samples became narrower with the introduction of Bi, indicating that Bi/$ZnSnO_3$ samples could be more effectively excited by visible light.

The band energy potentials of the prepared samples were determined using the Mott–Schottky (M–S) experiment. As shown in Fig. S2,† it can be seen that $ZnSnO_3$ showed the n-type semiconductor behavior from the positive tangent slope. The flat band (FB) potential of $ZnSnO_3$ was estimated to be −0.42 eV. It is well known that the conduction band (CB) position is generally lower than that of the FB by about 0.1–0.3 eV for the n-type semiconductor;[33,34] thus, the CB of $ZnSnO_3$ was determined to be −0.28 eV (*vs.* NHE). Based on the equation $E_g = E_{CB} + E_{VB}$, the VB position was calculated to be 2.92 eV, and the visualized energy band diagram is shown in Fig. 3C, indicating that the photo-generated holes had a strong oxidizing ability to satisfy the oxidation of NE.

PL spectra further confirmed the electron–hole separation efficiency. Fig. 3D shows the room-temperature PL spectra of the as-prepared samples. Notably, the emission peak intensity of the Bi/$ZnSnO_3$ samples was sharply diminished as the Bi content increased in comparison with pure $ZnSnO_3$, which demonstrated that the metallic Bi played an important role in the electron transfer, effectively inhibiting the recombination of photogenerated carriers, and then improving the PEC performance of Bi/$ZnSnO_3$ composites.

3.3. Electrochemical characterization

To some extent, the transient photocurrent reflects the separation efficiency of photogenerated electrons and holes and can be used to assess the photoelectric properties of the catalyst. The photocurrent responses of $ZnSnO_3$/FTO and Bi/$ZnSnO_3$/FTO were examined in a 0.1 mol L^{-1} Na_2SO_4 solution. As shown in Fig. 3E, $ZnSnO_3$/FTO generated a weak anodic photocurrent owing to the low carrier separation efficiency. After introducing the metallic Bi into the PEC system, it was apparent that the PEC responses of all Bi/$ZnSnO_3$/FTO increased more significantly than that of the pure $ZnSnO_3$/FTO, which indicated that the metallic Bi-modified $ZnSnO_3$ possessed excellent PEC performance and more effectively facilitated the separation and transfer of photogenerated electrons at the interface of composites.

EIS analysis was used to investigate the capability of the interfacial charge transfer using $[Fe(CN)_6]^{3-/4-}$ as a redox probe. It is well-known that the semicircle in the EIS curve stands for the charge transfer resistance (R_{ct}) between the electrode and the electrolyte, and the R_{ct} value is equal to the diameter of the semicircle. As shown in Fig. 3F, all Bi/$ZnSnO_3$/FTO showed lower resistance than the single $ZnSnO_3$/FTO, and Bi/$ZnSnO_3$-2/FTO displayed the lowest R_{ct} values. More importantly, the R_{ct} values of the modified electrodes were dramatically decreased under illumination conditions. It can be deduced that the combination of metallic Bi and $ZnSnO_3$ microspheres was beneficial for improving the conductivity of the electrode, accelerating the interfacial electron transport, and enhancing the PEC performance. However, excess Bi attached to the $ZnSnO_3$ surface may cover the surface voids of the microspheres and hinder sufficient contact between the electrode and the probe. Overall, the experiment results were as expected.

3.4. Highly sensitive PEC sensing of NE

To verify the feasibility of the Bi/$ZnSnO_3$-based PEC sensor for NE detection, several tests were conducted in the absence and presence of NE. When NE was added into the PEC system, it was easily oxidized by the photo-generated holes in the VB of the $ZnSnO_3$, and all of the modified electrodes displayed obvious enhancement of the anodic signal (Fig. 4A). Note that Bi/$ZnSnO_3$-2/FTO presented a remarkable photocurrent response, which was about 2.45-fold of that on $ZnSnO_3$/FTO, suggesting that Bi/$ZnSnO_3$-2/FTO had good sensitivity to NE, and the introduction of moderate metallic Bi would help to improve the detection sensitivity of NE. Excess Bi nanoparticles covering the $ZnSnO_3$ microspheres restricted the exposure of the surface Zn^{2+} sites, which was not conducive to the chelation interaction with target molecules, and the results were in agreement with the EIS analysis. Thus, with balanced properties, Bi/$ZnSnO_3$-2/FTO showed the best potential in the selective PEC sensing of NE.

After a series of experimental optimizations (Fig. S3†), the developed Bi/$ZnSnO_3$-2/FTO was utilized for NE determination. The transient photocurrent responses of Bi/$ZnSnO_3$-2/FTO with increasing addition of different concentrations of NE are shown in Fig. 4B. It can be seen that Bi/$ZnSnO_3$-2/FTO displayed an excellent and rapid photocurrent response to NE concentration, which demonstrated that more targets were captured by the electrode surface and participated in the PEC reaction, implying the fast interaction between NE molecules and the photoelectrode. As shown in Fig. 4C, the photocurrent increment value was proportional to the NE concentration in the range of 0.002–350.0 μmol L^{-1}, expressed by the following two regression equations: $\Delta I = 2.028c - 0.118$ ($R^2 = 0.995$, 0.002–10.0 μmol L^{-1}) and $\Delta I = 0.783c + 12.667$ ($R^2 = 0.998$, 10.0–350.0 μmol L^{-1}). The detection limit (LOD, 3S/N) was about 0.68 nmol L^{-1}, which is lower than those previously reported for modified electrodes (Table S1†), demonstrating better detection performance. In addition, the developed label-free PEC biosensor also exhibited higher sensitivity and lower LOD than the conventional electrochemical detection method (LOD = 4.2 nmol L^{-1}) (Fig. 4D). Such an excellent PEC sensing performance of Bi/$ZnSnO_3$-2/FTO was attributed to the fast carrier separation efficiency, large contactable area and unique interaction between the photoelectrode and targets, which

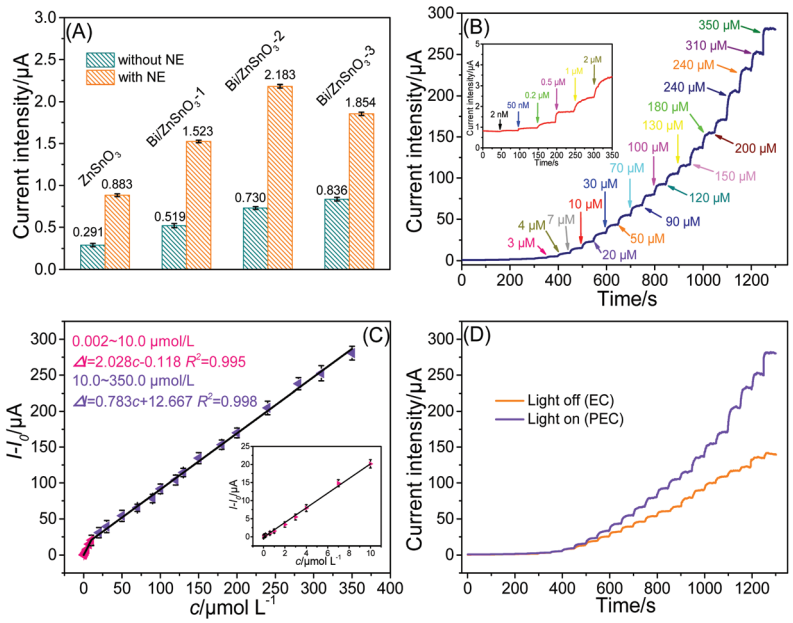

Fig. 4 (A) Photocurrent responses of $ZnSnO_3$/FTO and different Bi/$ZnSnO_3$/FTO samples recorded in 0.1 mol L^{-1} Na_2SO_4 with and without 1.0 μmol L^{-1} NE; (B) the amperometric responses of Bi/$ZnSnO_3$-2/FTO with different concentrations of NE; (C) corresponding calibration curve; (D) the amperometric responses of Bi/$ZnSnO_3$-2/FTO with different concentrations of NE under dark and illuminated conditions.

could serve as a promising sensor for monitoring NE molecules.

3.5. Highly selective PEC sensing of NE

In order to study the selective recognition ability of the proposed PEC sensor in depth, some catechol derivatives including EP and DA and other coexisting substances in biological fluids were chosen to investigate their influence on the response of Bi/$ZnSnO_3$-2/FTO. The results showed that only NE could cause a notable PEC response (Fig. 5A). As revealed in Fig. 5B, 2-fold DA, DOPA and EP, 5-fold CC and 30-fold UA, AA, L-Cys and L-tyrosine did not interfere with the photocurrent of NE, while 50-fold of other compounds such as glucose, urea, L-arginine, glutamic acid, glycine and galactose also showed a

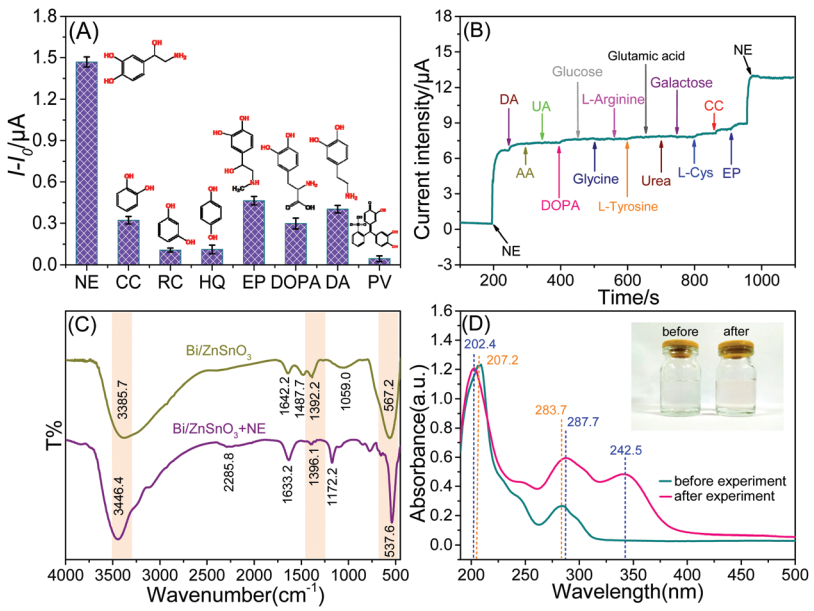

Fig. 5 (A) Photocurrent responses of different catechol derivatives on Bi/$ZnSnO_3$-2/FTO in 0.1 mol L^{-1} Na_2SO_4; (B) selectivity of Bi/$ZnSnO_3$-2/FTO; (C) FTIR spectra of Bi/$ZnSnO_3$-2 samples before and after adsorption of NE; (D) UV-vis spectra of the NE solution before and after the experiment; inset: photographs of the NE solution before and after the experiment.

negligible effect, reflecting an outstanding specificity towards NE analysis. This encouraged us to further analyze the underlying mechanism. Zn-based compounds might play a significant role in the selective determination of NE. The $ZnSnO_3$ photoelectrode (Zn^{2+}) can coordinate with the catechol structure to form a stable five-atom ring chelate for the selective detection of catechol derivatives; hence CC shows a higher PEC signal than resorcinol (RC) and hydroquinone (HQ), as shown in Fig. 5A. Among these derivatives, it was noted that EP was most likely to interfere with the determination of NE because they have similar structures, which can also chelate with the photoelectrode and produce a high PEC response. However, it is known that photogenerated holes preferentially react with targets with lower redox potentials.[35] Thus, we controlled the specific bias potential for the oxidation of NE (0.4 V) to avoid interference from EP (0.501 V). Accordingly, the current contribution from the oxidation of CC (0.527 V) and DOPA (0.482 V) would be negligible. Quite interestingly, PV and DA exhibited lower oxidation potentials (0.384 V and 0.369 V) than NE (Fig. S4†), and so should have higher photocurrents; but an abnormal phenomenon was observed where NE preferentially reacted. The reason for this phenomenon was probably that the electron-accepting group in PV may greatly suppress its ability to be oxidized. Compared to DA, the other two adjacent –OH and amino groups in the NE species may also coordinate with the surface Zn^{2+} site, resulting in the formation of two stable five-membered chelating ring structures, thus triggering a higher photocurrent than DA. The above results confirmed that the high sensitivity and selectivity of this PEC biosensor were ascribed to the appropriate control of the bias potential and unique chelating coordination interaction, showing the possibility of selectively monitoring NE in real samples.

Furthermore, to fully verify the interaction between NE and Bi/$ZnSnO_3$/FTO, FTIR and Raman analysis were carried out to reveal the underlying mechanism. As shown in Fig. 5C, the characteristic peaks of O–H and M–O–M groups in Bi/$ZnSnO_3$ at 3385.7 and 1392.2 cm^{-1} red shifted to 3446.4 and 1396.1 cm^{-1} after adsorption of NE, and the peak of M–O shifted from 567.2 to 537.6 cm^{-1}, which could be ascribed to the coordination between Bi/$ZnSnO_3$ and NE.[36] Moreover, Bi/$ZnSnO_3$ samples bonded with NE also showed additional infrared bands at 2285.8, 1633.2 and 1172.2 cm^{-1}, corresponding to the N–H, C=C and C–O stretching vibrations of NE,[37] respectively. Additionally, the Raman scattering peaks of Bi/$ZnSnO_3$ showed a red-shift after interaction with NE and two new, weak peaks near 1132 and 1497 cm^{-1} were recorded, which could be attributed to the vibrational modes of C–O and C=C bonds (Fig. S5†).[38] Both the FTIR and Raman results implied the variation of the local coordination environment after adsorption of NE and confirmed the chemical interaction between Bi/$ZnSnO_3$ and NE. Subsequently, UV-vis spectrophotometry was performed to analyze the NE solution before and after the PEC test (Fig. 5D). The results demonstrated that the absorption peak shape and position for the tested samples changed significantly compared to the original NE solution, indicating that NE was oxidized into new compounds. In agreement with the expected result, the color of the NE solution turned light pink after the PEC test (inset in Fig. 5D). Accordingly, we concluded that a label-free selective detection strategy for NE was achieved.

3.6. PEC mechanism of the biosensor

On the basis of these factors, the possible mechanism of the label-free Bi/$ZnSnO_3$-based PEC biosensor for the selective detection of NE is proposed, as shown in Scheme 1. Firstly, the incorporation of Bi enhanced the light absorption ability of $ZnSnO_3$ ranging from UV to near-infrared light, which helped to produce more active electrons and holes on the $ZnSnO_3$ surface. Upon light irradiation, the photo-generated electrons in the VB of $ZnSnO_3$ were excited to the CB, and the holes left in the VB. Since the Fermi energy of the metallic Bi (about −0.17 eV) was lower than that of $ZnSnO_3$, the photoexcited electrons on the CB of $ZnSnO_3$ would easily inject into the metallic Bi through the Schottky barrier. Furthermore, the closely anchored metallic Bi nanoparticles on the $ZnSnO_3$ surface could function as electron acceptors to facilitate the separation of electron–hole pairs and produced an enhanced anodic photocurrent signal, which was also confirmed by the open circuit potential (OCP) test. As shown in Fig. S6,† the OCP of Bi/$ZnSnO_3$-2/FTO was significantly decreased upon light irradiation, further indicating that Bi/$ZnSnO_3$ was an effective electron transport medium in the photoanode.[39,40] After adding NE to the PEC system, NE is identified by Bi/$ZnSnO_3$/FTO and forms a stable chelate with Zn^{2+} at the surface sites, further consuming the photo-generated holes to be oxidized. Simultaneously, the photo-generated electrons were eventually collected by the FTO substrate and entered the external circuit, resulting in an amplified anode photocurrent. Based on this, a sensitive and selective PEC sensor could be constructed considering the composition and interaction with target molecules.

3.7. Reproducibility, stability and application

To evaluate reproducibility, six PEC sensors were prepared using the same method as above for the determination of NE

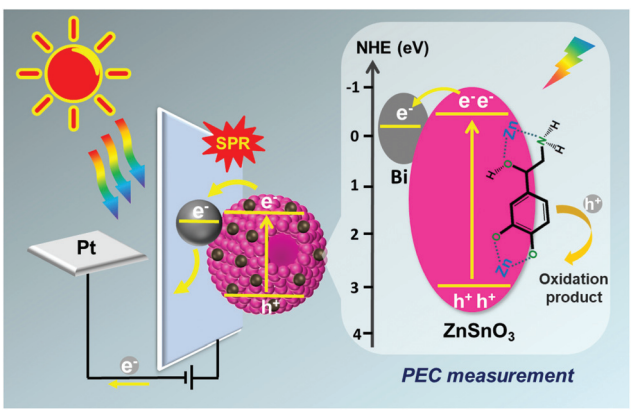

Scheme 1 Proposed mechanism of the label-free PEC biosensing platform for selective detection of NE.

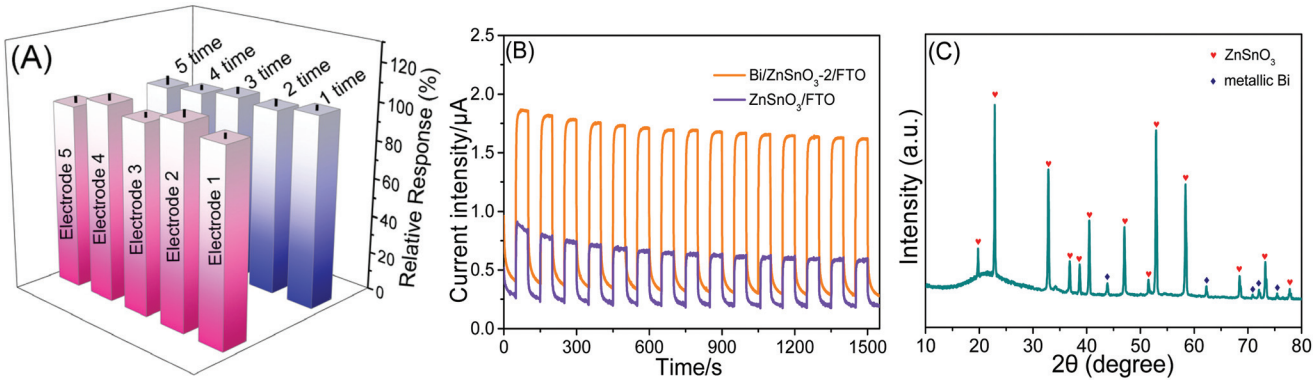

Fig. 6 (A) Photocurrent responses of five Bi/$ZnSnO_3$-2/FTO in the presence of 1.0 μmol L^{-1} NE and the repeated test of Bi/$ZnSnO_3$-2/FTO for five times, (B) the photocurrent stability of $ZnSnO_3$/FTO and Bi/$ZnSnO_3$-2/FTO in 0.1 mol L^{-1} Na_2SO_4 with 1.0 μmol L^{-1} NE; (C) XRD pattern of Bi/$ZnSnO_3$-2 after use.

(Fig. 6A). A relative standard deviation (RSD) of 3.2% was obtained. The repeatability was also evaluated by using the same sensors for five repeated analyses, with an RSD of 2.5%. The operational stability of Bi/$ZnSnO_3$-2/FTO was examined by 15 repeated "on–off" illumination cycles in the presence of NE. As shown in Fig. 6B, the photoelectrode exhibited a relatively stable photocurrent signal over the tested time range (1550 s), indicating outstanding stability of the electrode during the tests, while the signal attenuation of pure $ZnSnO_3$/FTO was obvious due to the rapid recombination of photoinduced electron–hole pairs. The used Bi/$ZnSnO_3$-2 samples were further examined by XRD (Fig. 6C), which confirmed the crystalline nature of Bi/$ZnSnO_3$ was not transformed, further proving the satisfactory test stability. In addition, the photocurrent signal of the prepared PEC sensor remained at 92.6% after storing for one week at room temperature. These results revealed that the proposed PEC sensing platform had an acceptable accuracy and stability.

Based on the excellent sensing performance of Bi/$ZnSnO_3$/FTO, the analytical applicability of the proposed sensor was evaluated for NE detection using human urine, human blood serum and injection samples as model systems. The urine sample was collected from healthy volunteers and the blood serum sample was obtained from the Shenyang First People's Hospital. These samples were centrifuged for 10 min at 4000 rpm and filtered through a 0.45 μm membrane; then, each filtrate was diluted 5-fold with the electrolyte solution. The unspiked samples were tested first, and the results obtained were in good agreement with the NE normal values.[41,42] Furthermore, the commercial NE injection (2.0 mg mL^{-1}) was bought from the local pharmacy. 10.0 μL of the initial NE injection was added to the electrolyte for direct detecting. Two different concentrations of NE were spiked into the above samples for recovery evaluation, and the results are listed in Table 1. These results clearly indicated that the recoveries were in the range of 93.8–106.0% and the RSD was between 2.8 and 4.5, indicating that there was no significant matrix interference, and this PEC biosensor was accurate and suitable for NE analysis in pharmaceutical and real samples, demonstrating its potential applicability and feasibility in clinical diagnosis.

Table 1 Analytical results of NE in the real samples using the proposed PEC biosensor

Samples	Added (μmol L^{-1})	Found[a] (μmol L^{-1})	Recovery%	RSD
Human urine	0.00	0.06	—	3.8
	2.00	2.18	106.0	3.1
	20.00	20.48	102.1	3.3
Human blood	0.00	0.001	—	4.1
	2.00	1.96	98.0	4.2
	20.00	20.93	104.6	3.1
NE injection 1	0.00	2.48	105.1	4.5
	2.00	4.55	103.5	3.2
	20.00	21.77	96.5	2.8
NE injection 2	0.00	2.25	95.3	4.3
	2.00	4.11	103.0	2.9
	20.00	20.81	93.8	3.1

[a] Mean of three measurements.

4. Conclusions

In summary, a novel label-free and visible-light-excited PEC sensing platform based on the 3D Bi/$ZnSnO_3$ Schottky junction was successfully exploited for highly sensitive and rapid NE detection. Based on the specific chelation and controlling the bias potential, the designed PEC biosensor with remarkable advantages of high selectivity can be directly applied for distinguishing NE from various catechol derivatives and other coexisting biomolecules. Specifically, the chelate interaction between Zn^{2+} at the surface sites and the adjacent –OH as well as amino groups in NE possessed the ability to form two stable five-atom ring structures, opening up a new selective sensing approach. The fabricated PEC biosensor demonstrated the accurate detection of NE and was successfully applied for

NE evaluation in real samples. More importantly, the proposed photoelectrocatalyst provided a new strategy for designing the "signal-on" label-free PEC sensing platform for monitoring NE in biological fluids for the diagnosis of diseases.

Author contributions

Yuanyuan Dong: conceptualization, methodology, investigation, data curation, formal analysis, writing – original draft. Chenxing Xu: investigation, validation. Lei Zhang: funding acquisition, writing – review and editing.

Conflicts of interest

The authors declare that they have no conflict of interest.

Acknowledgements

This project was supported by the National Natural Science Foundation of China (NSFC52072164) and the Liao Ning Revitalization Talents Program (XLYC1902066). The authors also thank their colleagues and other students who participated in this study.

References

1 Q. Liu, J. Kim and T. Cui, *Sens. Actuators, B*, 2020, **317**, 128181.
2 J. Peng, Q. Huang, Y. Liu, P. Liu and C. Zhang, *Sens. Actuators, B*, 2019, **294**, 157–165.
3 Y. Zhu, Z. Xu, K. Yan, H. Zhao and J. Zhang, *ACS Appl. Mater. Interfaces*, 2017, **9**, 40452–40460.
4 K. Zhao, X. Yan, Y. Gu, Z. Kang, Z. Bai, S. Cao, Y. Liu, X. Zhang and Y. Zhang, *Small*, 2016, **12**, 245–251.
5 S. Wang, F. Wang, C. Fu, Y. Sun, J. Zhao, N. Li, Y. Liu, S. Ge and J. Yu, *Anal. Chem.*, 2020, **92**, 7604–7611.
6 Y. Liu, R. Li, P. Gao, Y. Zhang, H. Ma, J. Yang, B. Du and Q. Wei, *Biosens. Bioelectron.*, 2015, **65**, 97–102.
7 K. Yan, Y. Liu, Y. Yang and J. Zhang, *Anal. Chem.*, 2015, **87**, 12215–12220.
8 L. Zhang, Y. L. Shen, G. C. Fan, M. Xiong, X. D. Yu and W. W. Zhao, *Microchim. Acta*, 2019, **186**, 284.
9 H. Wang, B. Zhang, F. Zhao and B. Zeng, *ACS Appl. Mater. Interfaces*, 2018, **10**, 35281–35288.
10 J. Chen, H. Huang, Y. Zeng, H. Tang and L. Li, *Biosens. Bioelectron.*, 2015, **65**, 366–374.
11 M. Mazloum-Ardakani, Z. Alizadeh, F. Sabaghian, B. Mirjalili and N. Salehi, *Electroanalytical*, 2019, **32**, 455–461.
12 N. Lavanya and C. Sekar, *J. Electroanal. Chem.*, 2017, **801**, 503–510.
13 K. J. Samdani, D. W. Joh, M. K. Rath and K. T. Lee, *Electrochim. Acta*, 2017, **252**, 268–274.
14 K. J. Samdani, J. S. Samdani, N. H. Kim and J. H. Lee, *Biosens. Bioelectron.*, 2016, **81**, 445–453.
15 T. Madrakian, E. Haghshenas and A. Afkhami, *Sens. Actuators, B*, 2014, **193**, 451–460.
16 K. Ghanbari and A. Hajian, *J. Electroanal. Chem.*, 2017, **801**, 466–479.
17 O. B. Ibrahim, M. A. Mohamed and M. S. Refat, *J. Mol. Struct.*, 2014, **1056–1057**, 13–24.
18 A. Maikap, K. Mukherjee, B. Mondal and N. Mandal, *RSC Adv.*, 2016, **6**, 64611–64616.
19 S. Sakthinathan, S. Kubendhiran, S. M. Chen, K. Manibalan, M. Govindasamy, P. Tamizhdurai and S. T. Huang, *Electroanalytical*, 2016, **28**, 2126–2135.
20 H. Yang, R. Cao, P. Sun, J. Yin, S. Zhang and X. Xu, *Appl. Catal., B*, 2019, **256**, 117862.
21 L. Zhou, J. Feng, B. Qiu, Y. Zhou, J. Lei, M. Xing, L. Wang, Y. Zhou, Y. Liu and J. Zhang, *Appl. Catal., B*, 2020, **267**, 118396.
22 Z. Li, X. Zhou, J. Yang, B. Fu and Z. Zhang, *ACS Appl. Mater. Interfaces*, 2019, **11**, 21417–21423.
23 J. Zhou, A. Zhou, L. Shu, M.-C. Liu, Y. Dou and J.-R. Li, *Appl. Catal., B*, 2018, **226**, 421–428.
24 Y. Pang, Y. Li, G. Xu, Y. Hu, Z. Kou, Q. Feng, J. Lv, Y. Zhang, J. Wang and Y. Wu, *Appl. Catal., B*, 2019, **248**, 255–263.
25 Y. Yu, C. Cao, H. Liu, P. Li, F. Wei, Y. Jiang and W. Song, *J. Mater. Chem. A*, 2014, **2**, 1677–1681.
26 D. Hu, H. Liang, X. Wang, F. Luo, B. Qiu, Z. Lin and J. Wang, *Anal. Chem.*, 2020, **92**, 10114–10120.
27 Y. Chen, L. Yu, Q. Li, Y. Wu, Q. Li and T. Wang, *Nanotechnology*, 2012, **23**, 415501.
28 J. Xiong, X. Li, J. Huang, X. Gao, Z. Chen, J. Liu, H. Li, B. Kang, W. Yao and Y. Zhu, *Appl. Catal., B*, 2020, **266**, 118602.
29 P. Yan, L. Xu, X. Cheng, J. Qian, H. Li, J. Xia, Q. Zhang, M. Hua and H. Li, *J. Electroanal. Chem.*, 2017, **804**, 64–71.
30 X. Huang, F. Guo, M. Li, H. Ren, Y. Shi and L. Chen, *Sep. Purif. Technol.*, 2020, **230**, 115854.
31 P. Yan, L. Xu, D. Jiang, H. Li, J. Xia, Q. Zhang, M. Hua and H. Li, *Electrochim. Acta*, 2018, **259**, 873–881.
32 Z. Wang, S. Yan, Y. Sun, T. Xiong, F. Dong and W. Zhang, *Appl. Catal., B*, 2017, **214**, 148–157.
33 X. F. Huang, Q. Shen, J. B. Liu, N. J. Yang and G. H. Zhao, *Energy Environ. Sci.*, 2016, **9**, 3161–3171.
34 X. Han, S. Heuser, X. Tong, N. Yang, X. Y. Guo and X. Jiang, *Chemistry*, 2020, **26**, 3586–3590.
35 F. Han, Z. Song, M. H. Nawaz, M. Dai, D. Han, L. Han, Y. Fan, J. Xu, D. Han and L. Niu, *Anal. Chem.*, 2019, **91**, 10657–10662.
36 Y. Liu, Z.-H. Yang, P.-P. Song, R. Xu and H. Wang, *Appl. Surf. Sci.*, 2018, **430**, 561–570.
37 I. A. Jankovic, Z. V. Saponjic, M. I. Comor and J. M. Nedeljkovic, *J. Phys. Chem. C*, 2009, **113**, 12645–12652.
38 M. L. Roldán, S. A. Centeno and A. Rizzo, *J. Raman Spectrosc.*, 2014, **45**, 1160–1171.

39 J. Li, X. Gao, B. Liu, Q. Feng, X. B. Li, M. Y. Huang, Z. Liu, J. Zhang, C. H. Tung and L. Z. Wu, *J. Am. Chem. Soc.*, 2016, **138**, 3954–3957.
40 G. K. C. dos Santos, F. G. S. da Silva, A. R. Ferreira, R. de Cássia Silva Luz and F. S. Damos, *Microchem. J.*, 2019, **148**, 424–432.
41 R. T. Peaston and C. Weinkove, *Ann. Clin. Biochem.*, 2004, **41**, 17–38.
42 F. D. Ferreira, L. I. Silva, A. C. Freitas, T. A. Rocha-Santos and A. C. Duarte, *J. Chromatogr. A*, 2009, **1216**, 7049–7054.